Monitoring of Thermal Degraded AC Machine Winding Insulation by Inverter Pulse Excitation

C. Zoeller, M.A. Vogelsberger, Th.M. Wolbank

***Abstract* –The demand for AC machines in traction applications fed by voltage source inverters is increasing. These highly efficient drives working near and even above their rated values are expected to operate for many years or even decades. Thus, condition monitoring is gaining a more important role. With focus in this work on outages due to deteriorated machine winding insulation an online monitoring method is presented to detect changes in the insulation strength. With the proposed method the insulation system state is assessed before an actual short circuit occurs, without the need for additional equipment or disconnection of the drive. The inverter is used as a source of excitation, by applying pulse sequences with different duration to enable high frequency excitation and analysis in a range suitable for the insulation condition monitoring. The evaluation of a change in the electrical strength of the insulation is made by analyzing the transient current responses measured with the built-in sensors of the inverter.**

Index Terms—AC machines; Current measurement; Insulation testing; Pulse width modulation inverters; Stators; Switching frequency

I. Introduction

In modern traction applications consisting of ac machines fed by voltage source inverters (VSI) a continuous operation over decades also under harsh environment is expected. Especially, the machine is exposed to high temperatures. Heavy and frequent load cycles increase stress to the system components. Condition monitoring is required to fulfill the key requirements of a safe and reliable drive. Thus, the knowledge of the health state of the individual components of the drive system is important and monitoring systems are required. In this work, the term monitoring is used placing special focus to the stator winding of the machine.

According to [1] and [2] the monitoring of the machine state is an important issue, as stator related faults are described as one of the most common faults. Different stresses like thermal, electrical, mechanical and environmental strain the insulation system and changes the insulating properties of the materials, which results in a loss in the dielectric strength. A detailed description of the effects and causes can be found in [3], [4].

The deterioration of the insulation usually is a slowly developing process in the first (pre-fault) stage and accelerates to e.g. inter-turn short circuit, which is an actual fault condition. The condition of the insulation winding system is typically assessed with different industrially well known methods and measurements, e.g. dissipation factor tan(δ) (tan(δ) tip-up), partial discharge (PD), polarization index (PI) or surface insulation resistance test (SIR). Most methods are either offline measurements or need the experience of the examiner [3]. Other methods described in [5] and [6] can be applied online with additional signal injection equipment.

The approach in this paper aims to detect imminent insulation degradation of the stator winding insulation system of the motor in a drive system without any additional signal injection source or sensor equipment. By using the inverter to generate a pulse sequence with specific frequencies and measuring the transient current response, which is taken for the insulation health state evaluation, the method meets the boundary conditions. With the opportunity of the observation of the insulation state during the operation or at least at startup or shutdown without disassembling of the drive, unexpected down times can be avoided and maintenance on demand scheduled. As a consequence, system reliability can be kept high.

II. Traction Drive – Main Components

With focus on systems with low-voltage ac traction drives the complete system consists of the main components, the machine, which is typically an induction machine as well as the cabling and the voltage source inverters, cf. Fig. 1. The inverter delivers the ability to control the angular velocity of the rotor shaft by supplying the stator winding with voltage of variable frequency/magnitude using the pulse width modulation (PWM).

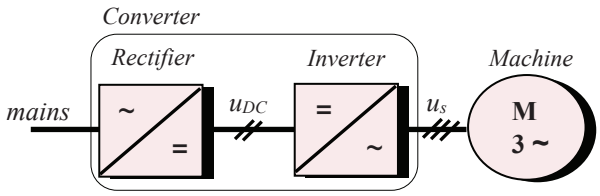

Fig. 1 Scheme of main components of a drive.

Currently, the voltage rise times due to switching of the power electronics are in the range of a few hundred nanoseconds. Due to newer upcoming wide-bandgap semiconductors, e.g. silicon carbide (SiC) or gallium nitride (GaN) significantly lower voltage rise times (higher dv/dt rates) are possible. In addition to the reduced incurred losses

The work to this investigation was supported by the Austrian Research Promotion Agency (FFG) under project number 83 84 78.

C. Zoeller is with the Institute of Energy Systems and Electrical Drives, Vienna University of Technology, 1040 Vienna, Austria (e-mail: clemens.zoeller@tuwien.ac.at).

M.A. Vogelsberger is with Bombardier Transportation Austria GmbH, Internal Supply Chain (ISC); Drives, 1220, Vienna, Austria (e-mail: markus.vogelsberger@rail.bombardier.com).

Th. M. Wolbank is with the Institute of Energy Systems and Electrical Drives, Vienna University of Technology, 1040 Vienna, Austria (e-mail: thomas.wolbank@tuwien.ac.at).

978-1-5090-2538-1/16/$31.00 ©2016 IEEE

in the inverter during a switching transition, the steep voltage flanks generate surges within the system inverter-cabling-stator winding through reflection and oscillations. Through the reflection phenomena the occurring overvoltages at machine terminal side reach up to 2 p.u. of the inverter output voltage according to [7] and up to 4 p.u. according to [8], depending on different factors, e.g. cable length, voltage rise time, switching transition etc.. These increased voltage levels additionally strain the insulation system of the machine winding.

The highest overvoltages occur at the stator winding terminals. This is explained by the value of the reflection coefficient 'Γ' of equation (1), which is the parameter that describes, how much of an electromagnetic wave is reflected by an impedance discontinuity. Due to impedance mismatch between the cabling (impedance Z_C) and the inverter (impedance Z_{Load} =Z_{In}), the reflection coefficient is about $\Gamma = -1$ due to $Z_{In} << Z_C$. The machine winding on the other hand provides for the rapid propagated pulse a very high impedance $Z_C << Z_{Ma}$ where Z_{Ma} is the characteristic impedance of the machine. The reflection factor is thus accordingly $\Gamma = +1$.

$$\Gamma = (Z_{Load} - Z_C)/(Z_{Load} + Z_C) \quad (1)$$

In addition to the reflection phenomena of the voltage, a transient decaying oscillation is also visible in the current trace after the switching transition. Investigations from the authors in [9] with accelerated aging of insulation systems in a stator slot model by applying thermal exposure, show the effects of degraded insulation during the aging process in connection with deviation in the current response after voltage step excitation. Additionally, in accordance with [10], the results show that one of the main parameters that is linked with insulation degradation is the measurable insulation capacitance, as this would be important in the later section.

In the following two sections the system components inverter and machine are described more in detail. For the cabling between the inverter and machine, 6m of standard industrially assembled power cables are used in all investigations in this work.

A. *Inverter*

The inverter used for the measurements in this work consists of four 4,7μF capacitors building the dc link and three IGBT half-bridges (cf. Fig. 2) designed for a maximum V_{CE} voltage of 1200V and rated current I_{rms} of 50A. Since the switching and delay times are important for these investigations, a clear definition in alignment with the typical denotation is given as follows. The turn on time of one IGBT-module is about 140ns and is defined by the sum of $t_{d(on)}$ (time from 10% of gate-to-emitter voltage V_{GE} to 10% of collector current I_c, about 80ns) and t_r (rise time from 10% of I_c to 90% of I_c, about 60ns). In contrast to the turn-off case with 460ns the time is defined by $t_{d(off)}$ (duration between 90% V_{GE} and 90% I_c, about 400ns) and t_f (fall time from 90% I_c to 10% I_c, about 60ns).

Another timing issue is the dead-time. If one IGBT is turned on, the other IGBT of the half-bridge cannot be switched. A digitally adjustable dead-time is generated by the gate drive unit, which has to be longer than the turn-off delay time of the IGBT. This avoids that one IGBT is turned on, before the other one is completely turned off. Due to safety reasons and the above mentioned timing values (depending on the load), the inter-lock dead time is set to 2μs for all measurements of this work.

B. *Machine*

The machine is a 5.5kW induction machine with a random-wound winding system. In the stator system round enameled copper wire is used, which is a winding wire according to EN13601 Cu-ETP with insulation consisting of polyesterimide and polyamide-imide as the over coat. The materials ensure a thermal durability and overload stability and are classified with thermal class H according to IEC 60085 (class 180 – IEEE definition). The resin is single component, monomer and volatile organic compound (VCO) free, based on specially modified unsaturated polyester. The thermal classification is also specified with class H (class 180). The conductors to the terminal block and the tapes are classified with class F (class 155).

As depicted in Fig. 2, the machine winding can be modeled by its fundamental wave parameters R_S (stator resistance) and L_S (stator inductance). Besides, these components the parasitic winding parameters , i.e., winding-to-ground capacitance $C_{Wdg\text{-}Gnd}$, phase-to-phase capacitance $C_{Ph\text{-}Ph}$ and turn-to-turn capacitance $C_{t\text{-}t}$ exist, which largely influence the high frequency behavior and consequently the transient overvoltages at the machine terminals.

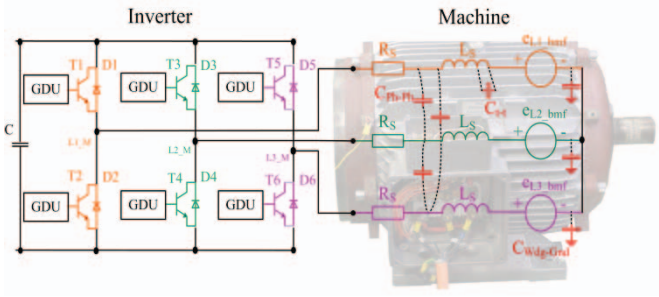

Fig. 2 Three half-bridge inverter and equivalent circuit diagram of 5.5kW induction machine.

III. Measurement Procedure and Insulation Degradation

A. *Excitation methods*

Basic idea of the proposed insulation health state estimation method is that in a specific high frequency range the machine is excited clearly above the machine's fundamental wave that is linked with the mechanical speed and typically does not exceed 1kHz. The high frequency excitation is realized with the inverter by a series of short switching transitions, as depicted in Fig. 3 (a). The figure depicts the measurement of the machine terminal L1 voltage with respect to lower dc-link voltage level. For this representation 50 consecutive measurements are performed

and in the enlarged area the mean signal, standard deviation and minimum/maximum values of one part of the signals are depicted.

In Fig. 3 (b) the machine's current reaction, resulting from the applied voltage excitation is depicted. The necessary excitation frequency of the voltage pulses for the insulation monitoring depends on the insulation system and the construction of the machine. For machines with rated power of up to 100kW and random wound stator winding the range is typically from 10kHz to 6MHz. In case of pre-formed stator coils and machines with higher rated power of MW and above, the frequency range is typically from 10kHz to 2MHz.

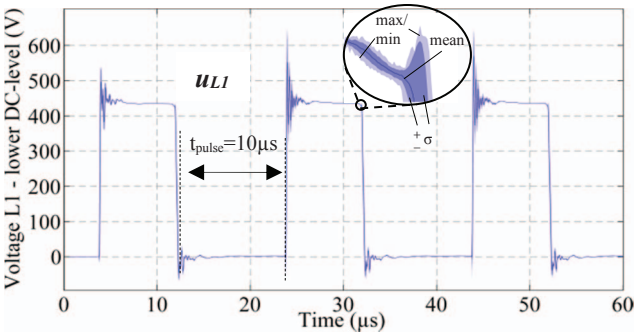

(a)

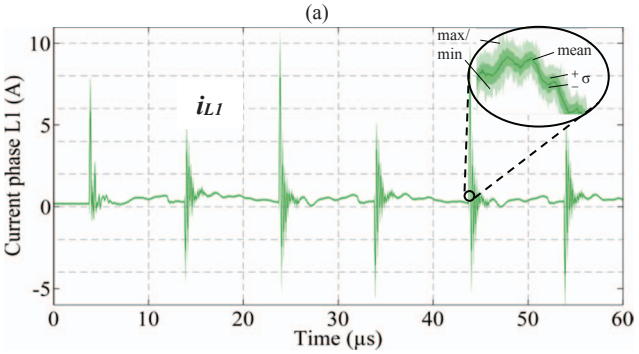

(b)

Fig. 3 (a) Machine terminal voltage L1 with respect to lower dc-link voltage, (b) current reaction in phase L1.

Regarding currently available industrial inverters, the minimal duration for voltage pulses is limited to few microseconds. This leads to excitation frequencies in the lower portion of the frequency range suitable for insulation degradation monitoring. The measurements in this work are limited to a maximum excitation pulse frequency of 166 kHz. However, with new power semiconductor technology, e.g. silicon carbide (SiC) or gallium nitride (GaN), higher switching frequencies are reachable, that cover also the upper portion of the aforementioned frequency range for the different machine types.

B. Inverter interlock-dead time influences

The challenge at modern industrial inverters is that they are not designed to continuously apply a pulse sequence in the frequency range of several hundred kHz. In order to keep the incurred switching losses low, a sequence of only few 6 very short pulses is used in the presented investigation and specific excitation frequencies (12.5kHz, 25kHz, 50kHz, 83,3KHz and 166,6kHz).

Due to inverter interlock-deadtime and other non-ideal properties of the inverter, the actual voltage excitation signal gets distorted leading to additional excitation frequencies. In addition, resulting from the impedance mismatch of inverter, cable and machine, reflections of the voltage wave occur, leading to distinctive higher harmonics.

In Fig. 4 (a) and (b) a scheme of a switching transition of one half bridge in dependence from the current flow direction is depicted. In the left subfigure a transition from upper to lower as well as lower to upper transistor is depicted with positive current direction. In case of the switching transition from the upper to the lower transistor (a – dashed blue arrow), the machine current commutates immediately after turn-off of the upper transistor by the gate drive unit to the freewheeling diode. Therefore the output terminal obtains the negative dc-link potential immediately and dead time does not influence the output voltage trace. In contrast to a switching transition from lower to upper transistor, indicated by the dashed red arrow. In this case the lower freewheeling diode was conducting before the switching transition and thus turning off the bottom transistor does not affect the output voltage. After expiration of the dead time, the upper transistor is turned on and the output terminal assumes positive intermediate circuit potential. In this case, the change in the voltage trace is delayed.

In subfigure (b) the effect of the dead time on a switching transition during negative current direction is depicted.

In subfigure (c) the effect on the current trace is depicted in case of positive and negative current. The alternating decrease or increase of the pulse duration is indicated with t_{pulse}-Δt_d and t_{pulse}+Δt_d.

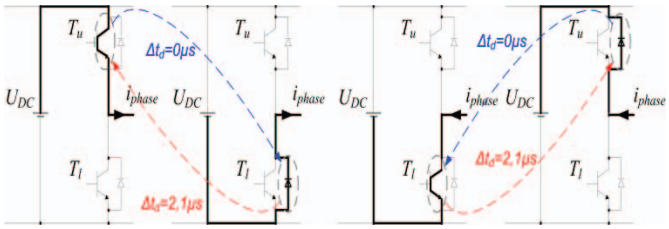

(a) (b)

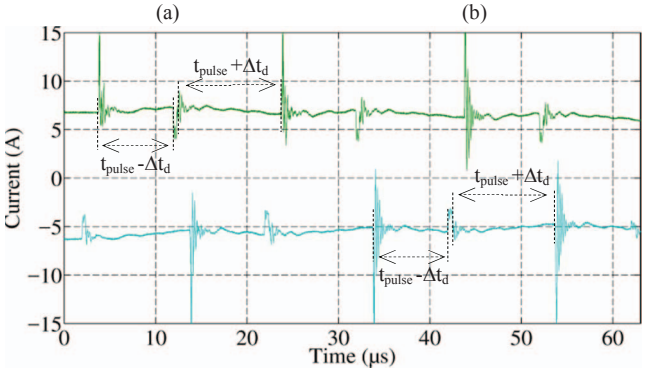

(c)

Fig. 4 (a,b) Scheme of switching transition in dependence of current flow direction and acting dead time (c) current trace according to the inverter dead time for t_{pulse}=10µs.

C. Spectral components of excitation signal

The special voltage pulse sequence of Fig. 3 (a) with a specific dominating frequency of 50kHz is realized by time-shifted voltage space phasors pointing in opposite direction of one phase (in this case the sequence L1+, L1-, L1+, L1-,

L1+, L1-) with a duration of 10µs for each single pulse. Furthermore, due to the dependency on the type of insulation system and divergence from machines of the same type the interesting frequency range for the insulation monitoring process may span over a wide range. As can be seen in Fig. 3 (a) the voltage excitation signal is of trapezoidal shape, the spectrum and thus the excitation frequencies depending on the various rise times and duty cycles, illustrated in Fig. 5 (a). The Fourier analysis on the time signal *x(t)* with equation (2), results in the coefficients given with expression (3), with the approximation that the rise time T_R is equal to the fall time T_F.

$$c_v = \frac{1}{T}\int_{t_0}^{t_0+T} f(t)\, e^{-jv\omega_0 t}\, dt \tag{2}$$

$$= A\frac{T_P}{T}\, sinc\left(v\omega_0\frac{T_P}{2}\right) sinc\left(v\omega_0\frac{T_R}{2}\right) e^{-j\omega_0\frac{(T_P+T_R)}{2}} \tag{3}$$

The envelope of the excitation signal is given by the two '*sinc'* functions, which delivers the upper bound in the spectrum of the coefficients in a logarithmic frequency plot, cf. in Fig. 5 (b).

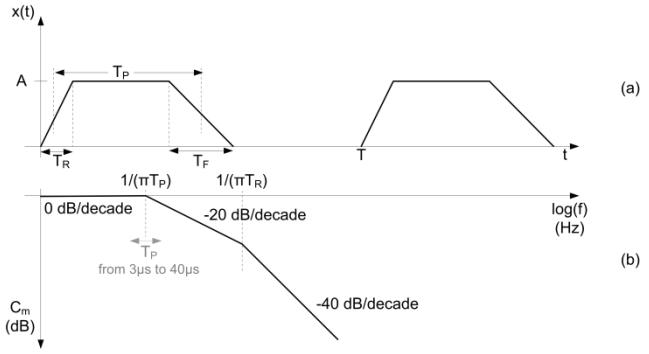

Fig. 5 (a) Time signal of trapezoidal shape, (b) spectrum of envelope.

If the duty cycle is short enough that the frequency $1/(\pi T_P) > 2\pi/T$ is bigger than the fundamental frequency the spectrum starts with a 0dB/decade. The term $sinc(v\pi f T_P)$ results in a asymptote with a slope of -20dB/decade, until the second border frequency $1/(\pi T_R)$ defined by $sinc(v\pi f T_R)$ depending on the rise time T_R. As can be seen the energy of the signal is spread over a broad range of frequencies and with variation of the pulse width T_P (in this work 3μs, 6μs, 10μs, 20μs and 40μs) the trace can be shifted and different frequencies can be considered for the monitoring process.

D. Insulation monitoring

For the insulation monitoring the signals are analyzed in the frequency range. Fig. 6 (a) and (b) depicts the amplitude spectrum of the voltage excitation signal Y_U and corresponding current reaction of Fig. 3 (a) and (b) calculated with equation (4)- the discrete Fourier transform. For the sake of clarity, the discrete frequency points are represented with a curve.

$$Y[k] = \sum_{n=0}^{N-1} y[n] e^{-j\left(\frac{2\pi}{N}\right)nk}\ , k = 0, \dots, N-1 \tag{4}$$

As can be seen in the upper subfigure the target frequency with a pulse duration of t_{pulse}=10µs is f_t=50kHz (red dashed line), however the actual main excitation frequency is f_a=43,96kHz. In Fig. 6 (b) the amplitude spectrum of the current reaction due to the inverter excitation is measured in phase L1 with a Rogowski-coil, denoted with $Y_{I1}[k]$, with a specified bandwidth of f_{3dB}~16MHz and in case of the built-in standard industrial current transducers of the inverter, denoted with $Y_{I2}[k]$, with f_{3dB}~150kHz and di/dt~50A/µs. It is clearly visible that the main excitation frequency is accurately detected by the Rogowski-coil. In case of the current transducer additional frequency components strengthened occur due to the internal structure of the sensor. However, despite the response to the excitation procedure depending on the sensor characteristic, the response is still reproducible and can thus be compared to initial measurements taken at a new insulation system.

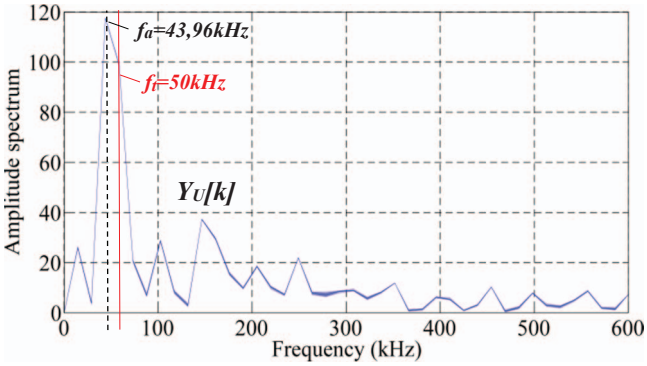

(a)

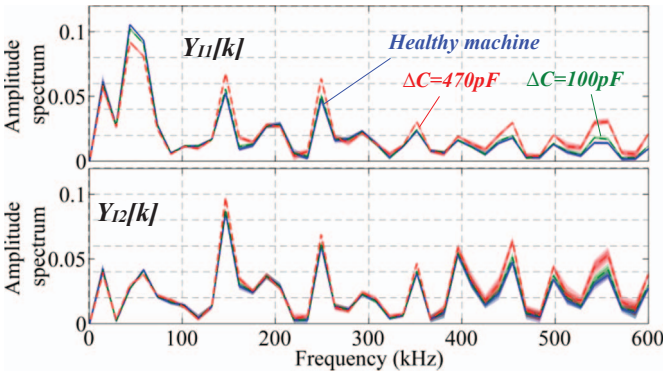

(b)

Fig. 6 (a) Amplitude spectrum of voltage pulse excitation signal (t_{pulse}=10µs) with actual excitation frequency f_t=50kHz and target frequency f_a=43,96kHz. (b) Amplitude spectrum of corresponding current reaction (current transducer f_{3dB}~150kHz and rogowski coil f_{3dB}~16MHz) for different machine states. (Healthy insulation state – blue; ΔC=100pF//L1 - green; ΔC=470pF//L1 - red)

Further, due to changes in the parasitic capacitances, resulting e.g. from degradation of the insulation system, a deviation in the machine's current response on the excitation is visible in a specific frequency range. When comparing the results obtained from a healthy machine with healthy insulation system and repeated measurements taken in service during specified intervals, a distinct change is detectable. The different degradation levels of the insulation system in Fig. 6 (b) are emulated with capacitors with different values (100pF and 470pF) placed in parallel to phase L1. Each of the traces represent the distribution of 50 single measurements and deviations between the healthy machine (blue trace) and degraded insulation scenarios

(green and red traces) are clearly observable over the depicted frequency range.

In practical applications, time intervals between the insulation state assessments can be in the range of a few hours in harsh operating conditions and up to several weeks in applications with low additional stress. As it was shown in [9], the measurable capacitance value of the insulation system decreases during the aging process and a capacitor parallel to the winding increases the total capacitance. However the used method gives evidence which deviations and dimensions of capacitance variations are detectable.

E. Accelerated aging

To analyze a change of the winding insulation system state the test machine has been aged by accelerated aging cycles until the failure of the insulation was determined with a voltage withstand test. Thermal aging by heating the machine winding with an oven to a defined temperature above the maximum approved level plays an important role for investigations regarding insulation degradation. High temperature in modern insulations leads to chemical reactions if exposed to temperatures above a threshold value. Through oxidation the insulation materials become brittle and tend to delamination in bandaged coil insulation types. In first approximation the rate of reaction of the oxidation process is given by the Arrhenius respectively by the Van 't Hoff equation, stating that the deterioration of an insulation increases by the factor 4 for each temperature increase by 20K. With equation (5) the life span L (in hours) of the insulation strength is estimated. The Factor E_a (activation energy), k_B (Boltzmann constant) and A (pre-exponential factor) can be assumed as constant. The equation is only valid for high temperatures above a specific threshold different for each insulation material. Due to the fact that more than one chemical reaction usually occur this formulation is not strictly valid.

$$L = Ae^{\frac{-E_a}{k_B T}} \tag{5}$$

The aging test procedure is established in accordance with the IEEE standard 1107-1996 [11]. By conducting heat exposures in repeated cycles, thermal deterioration effects are analyzed on an accelerated basis. Temperature and exposure period were chosen with the target to reach up to maximum ten cycles until failure of the insulation system is validated. The insulation system of the machine is classified with class F (class temperature ϑ_F=155°C) and the over temperature was set to ϑ_{aging1}=220°C with an exposure period of 2 days/cycle.

In Fig. 7 the test machine stator is shown after different aging cycles. The first two figures show the whole stator winding with the iron body and the enlarged winding overhang for the healthy machine state denoted with *'Cycle 0'*.

After three aging cycles are applied the figures in the middle row indicates that the machine winding suffers under the thermal aging, denoted with *'Cycle 3'*. As can be seen, the resin dissolves from the winding. The insulation tapes become also very brittle and the color gets dimmed. The enamel winding insulation of the coils has hardly changed. The withstand voltage test is carried out successfully at this state.

After nine aging cycles the resin has completely dissipated. The tapes crumble at contact and enamel insulation has small local defects as can be seen in the two lower figures of Fig. 7 (*'Cycle 9'*). The withstand test conducted with a voltage of 1kV failed at that state of the investigations.

Fig. 7 ASM 5.5 kW stator after different aging cycles.

With a frequency response analyzer (FRA), a non-destructive and sensitive method, the capacitance change due to the applied aging cycles is evaluated. By injection of low voltage sinusoidal signal constant in amplitude but with increasing frequency sweep the impedance of a test specimen winding over a wide frequency range is analyzed and compared to the result with a reference set. In Fig. 8 the capacitive change of phase L1 is depicted in a frequency range from 10kHz to 100kHz. At the observed frequency range the deviation from the reference (blue trace - *'Cycle 0'*) to the last applied aging cycle (gray trace *'Cycle 9'*) is about ΔC~25%.

IV. Insulation State Assessment

In this section the implementation of the aforementioned facts is shown to obtain an in service monitoring process.

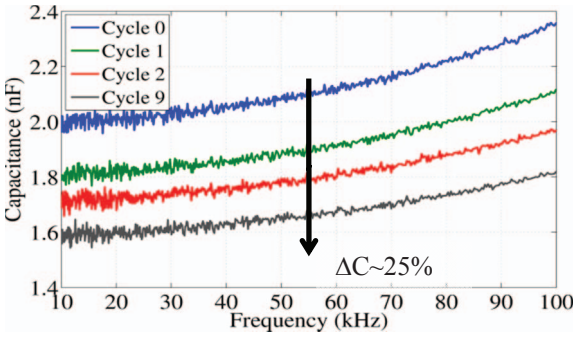

Fig. 8 Tendency of capacitive change of phase L1 measured by frequency response analyzer FRA.

The aim of the insulation monitoring by varied inverter pulse excitation is to detect imminent insulation degradation, which evolves usually slowly after unspecified time of operation. Furthermore, various insulation components (turn-turn insulation, groundwall insulation etc., cf. Fig. 2) can be affected by aging and the effect on the transient current response is impacting differently. Thus, the observation of a change over a wide frequency range is advantageous. Therefore a frequency range up to 1MHz is analyzed and the severity of the insulation degradation is assessed by root mean square deviation (RMSD) calculated from the difference of the healthy machine state spectrum and spectra of further measurements after each aging cycle. The resulting value is denoted as the *Frequency Response Deviation* (FRD). With equation (6) a value for the actual machine state is calculated.

$$FRD_p = RMSD_p(x_1, x_2) = \sqrt{\frac{\sum_{i=1}^{n}\left(Y_{ref,p}(f_i) - Y_{con,p,n}(f_i)\right)^2}{f_{range}}} \qquad (6)$$

In order to ensure statistical interpretation of the data one machine insulation state is represented by a high number of consecutive measurements. These measurements are taken in a sequence and in this work the number was set to 50 measurements. For the representation of the healthy machine state a reference current amplitude spectrum $Y_{ref,p}$ is formed out of the 50 different spectra. The index p identifies the investigated phase. The second variable, denoted with $Y_{deg,p,k}$ represents the current amplitude spectrum of the emulated insulation degradation measurement. The index n represents the consecutive number of the repeated measurement. The variable f_{range} depends on the length of the observed frequency range.

In Fig. 9 the calculated indicators after each aging cycle for the phase *L1*, *L2* and *L3* of the test machine in case of a pulse excitation with t_{Pulse}=6μs are depicted. The value at *'Cycle 0'* corresponds to mean of the healthy machine state compared with the individual measurements of the healthy machine states. Between the value of *'Cycle 0'* and *'Cycle 1'* there is a larger step merging into a saturation with small monotonic increasing tendency until *'Cycle 7'*, illustrated by the dashed gray line with the percentage change rates with respect to the healthy machine. There is a correlation between the insulation degradation detectable with the decreasing capacitance value of the winding system and the increasing tendency of the indicators observable for all three phases. At *'Cycle 8'* the voltage withstand test (1000V dc) failed for phase *L3* for the first time. Investigations showed that the winding passed a withstand test with lower voltages of several hundred volt, thus enabling inverter-fed operation at rated dc-link voltage. Phase *L1* and *L2* passed the 1kV dc test successfully. The change in the insulation state of phase *L3* affects the current response of the two other phases, visible with the high indicator values in all three subfigures. After '*Cycle 9*' the winding insulation tests completely failed. However, it was still possible to continue at *'Cycle 8'* and *'Cycle 9'* with inverter operation (test pulses) with nominal voltage. It is suggested that the ground leakage currents in these two states were still very small and the results can be concluded as a scenario of a badly damaged insulation in a state just before an actual failure of the machine.

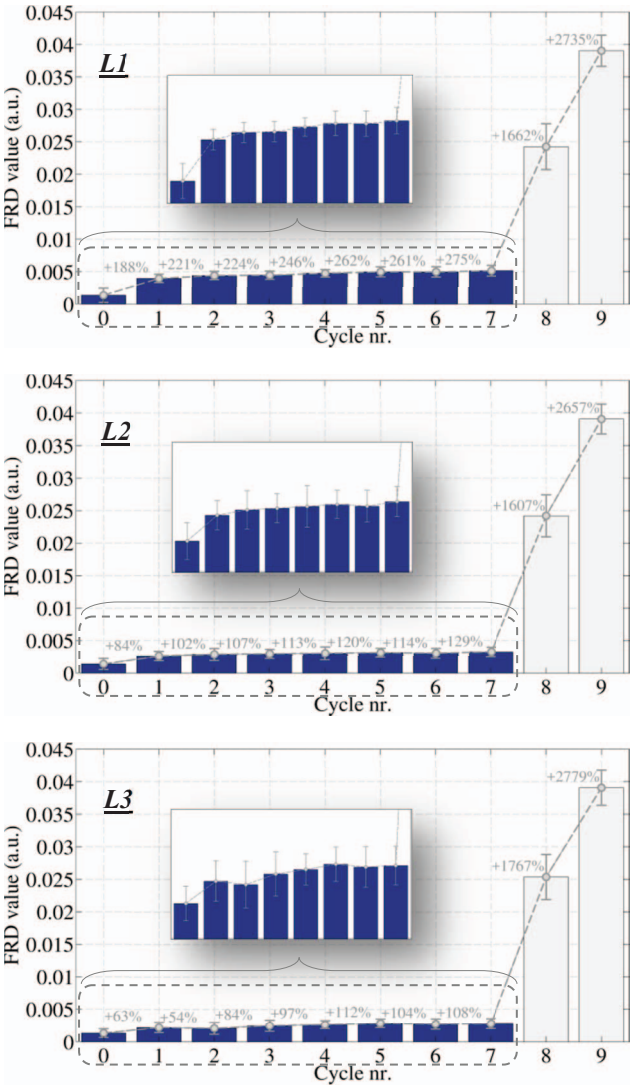

Fig. 9 Insulation state indicators for phase L1- L3 for each aging cycle.

Fig. 10 depicts the current reaction of phase *L3* in case of the healthy machine state at *'Cycle 0'* and after insulation degradation occurred in a final state of *'Cycle 8'*.

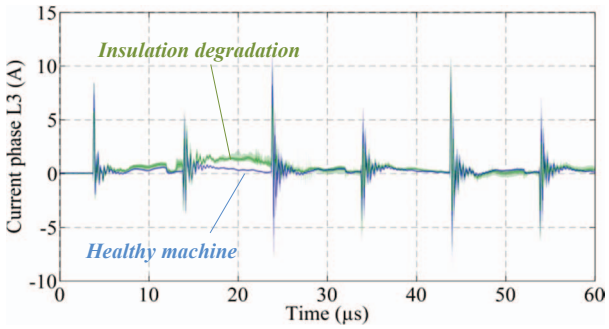

Fig. 10 Current response of phase L3 for healthy machine state (blue trace) and in case of insulation degradation (green trace).

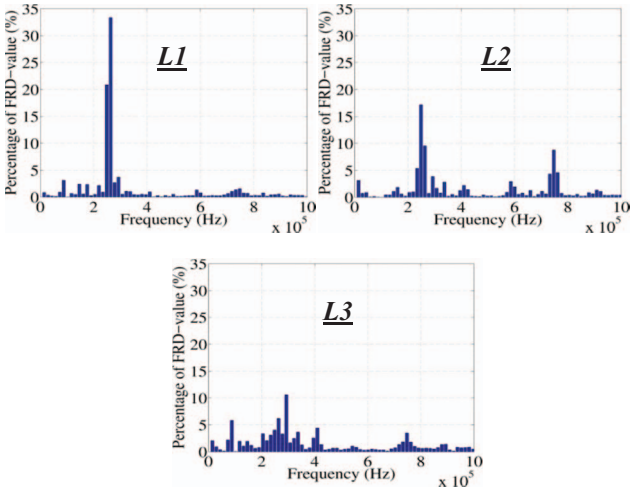

Fig. 11 Fraction in percentage of the deviations on the indicator at each equidistant frequency point.

Due to economic reasons the usage of a lower ADC sampling rate is preferred. Thus, the selected frequency range for the indicator calculation was limited to a maximum frequency of 1MHz. In Fig. 11 the fraction of the calculated deviation of the Fourier coefficients from the healthy state in percentage at each equidistant frequency within the observation range are depicted. The values represent the mean values of the cycles 0-7. As can be seen from Fig. 11 the frequency range between 200-350kHz is most sensitive to changes in the insulation health state for the considered test machine. Due to limitation in the power electronics devices, maximum frequency of the main pulse excitation was around 160kHz. Thus, a direct main pulse excitation within the most sensitive frequency (200-350kHz) was not possible so far.

V. Conclusion

A new method to detect insulation degradation has been proposed. It is based on the frequency response of the machine current to a voltage excitation with a specific dominant frequency. The excitation is established by a voltage pulse sequence of the inverter having a dominant fundamental wave that equals the target excitation frequency. The current response is measured with standard industrial sensors as well as Rogowski type sensors. One advantage of the method is that the main excitation frequency can be changed to cover the frequency range of the machine, most sensitive to changes in the winding insulation health state by changing the frequency of the pulse sequence. Thus a frequency response trace of the machine insulation can be estimated. Monitoring the insulation health state, down times can be avoided and maintenance on demand scheduled.

VI. Acknowledgment

The work was supported by the Austrian Research Promotion Agency (FFG) under project number 838478.

VII. References

[1] IEEE Committee Report, “Report of large motor reliability survey of industrial and commercial installation, Part I,” *IEEE Transactions on Industry Applications*, vol.21, no.4, pp.853–864, 1985.

[2] IEEE Committee Report, “Report of large motor reliability survey of industrial and commercial installation, Part II,” *IEEE Transactions on Industry Applications*, vol.21, no.4, pp.865–872, 1985.

[3] Stone, G. C.; Boulter, E. E.; Culbert, I.; Dhirani, H., “Electrical Insuation for Rotating Machines”. *IEEE Press*, 2004.

[4] Toliyat, H. A., et al. “Electric Machines: Modeling, Condition Monitoring, and Fault Diagnosis”. *CRC Press*, 2012.

[5] Neti, P.; Grubic, S., "Online broadband insulation spectroscopy of induction machines using signal injection," 2014 IEEE Energy Conversion Congress and Exposition (ECCE), pp.630-637, 14-18 Sept. 2014.

[6] Perisse, F.; Werynski, P.; Roger, D., “A New Method for AC Machine Turn Insulation Diagnostic Based on High Frequency Resonances,” IEEE Transactions on Dielectrics and Electrical Insulation, vol.14, no.5, October 2007.

[7] Knockaert, J.; Peuteman, J.; Catrysse, J.; Belmans, R., "Hidden reflection phenomena on inverter-fed induction motors," 2005 European Conference on Power Electronics and Applications, pp.9 pp.-P.9, 11-14 Sept. 2005.

[8] Amarir, S.; Al-Haddad, K., "Mathematical analysis and experimental validation of transient over-voltage higher than 2 per unit along industrial ASDM long cables," IEEE Power Electronics Specialists Conference, pp.1846-1851, 15-19 June 2008.

[9] Zoeller, C.; Vogelsberger, M.A.; Fasching, R.; Grubelnik, W.; Wolbank, T.M., "Evaluation and current-response based identification of insulation degradation for high utilized electrical machines in railway application," *2015 IEEE 10th International Symposium on Diagnostics for Electrical Machines, Power Electronics and Drives (SDEMPED)*, pp.266-272, 1-4 Sept. 2015.

[10] Farahani, M.; Gockenbach, E.; Borsi, H.; Schäfer, K.; Kaufhold, M., “Behavior of machine insulation systems subjected to accelerated thermal aging test,” *IEEE Transactions on Dielectrics and Electrical Insulation*, vol.17, no.5, 2010.

[11] IEEE Recommended Practice for Thermal Evaluation of Sealed Insulation Systems for AC Electric Machinery Employing Random-Wound Stator Coils," *In IEEE Std 1107*, 1996.

VIII. Biographies

Clemens Zoeller received the B.Sc. degree in Electrical Engineering and the M.Sc. degree in Power Engineering from Vienna University of Technology, Vienna, Austria in 2011 and 2013, respectively. He is currently Project Assistant at the Department of Energy Systems and Electrical Drives, Vienna University of Technology and working towards his PhD degree. His special fields of interest are fault detection, condition monitoring and sensorless control of inverter-fed AC machines.

Markus A. Vogelsberger received the the Dipl.-Ing./M.S. (with honor) and Dr.Techn/Ph.D. (with honor) degrees in Electrical Engineering from Vienna University of Technology, Vienna, Austria, in 2004 and 2009, respectively. He has been a Scientific Research Assistant in the Institute of Electrical Drives and Machines, Vienna University of Technology, where he has been engaged in several industrial and scientific R&D projects in the field of sensorless control, drives systems and power electronics / drive converter. In 2011, he joined Bombardier Transportation, Vienna, Austria.

Thomas M. Wolbank received the doctoral degree and the Associate Prof. degree from Vienna University of Technology, Vienna, Austria, in 1996 and 2004, respectively. Currently, he is with the Department of Energy Systems and Electrical Drives, Vienna University of Technology, Vienna, Austria. He has coauthored more than 100 papers in refereed journals and international conferences. His research interests include saliency based sensorless control of ac drives, dynamic properties and condition monitoring of inverter-fed machines, transient electrical behavior of ac machines, and motor drives and their components and controlling them by the use of intelligent control algorithms.